

High Speed Pupillometry

Shiau Shing Sammy Phang, D. Robert Iskander, and Michael J. Collins

Contact Lens and Visual Optics Laboratory, School of Optometry,

Queensland University of Technology, Australia.

(s.phang)(d.iskander)(m.collins)@qut.edu.au

Abstract

Measuring the parameters of the pupil in the human eye has become increasingly important in customised refractive surgery and other eye care applications. High-speed and high-resolution CMOS cameras can be used to study the dynamics of eyelids and their interaction with the pupil at different illumination levels. We consider the problem of measuring the pupil size from a high-speed video. In particular, we develop a novel algorithm for setting intra-lid sectors for the detection and estimation of the pupil and iris outlines from a sequence of digital images. An application of the proposed methodology to the estimation of the pupil parameters during an eye blink is given.

1. Introduction

In the past, the pupil size was often measured with a ruler or a special gauge. However, in the era of advanced refractive surgery and contact lens fitting, the traditional measurement techniques are not sufficient [1]. In many optometry and ophthalmology applications, it is important to determine the location of the pupil with respect to other features of the anterior eye such as the limbus (iris outline). For example, determining the relation between the pupil and limbus centres is crucial in corneal transplantation [2]. Also, in some surgical procedures there is a need to determine the pupil and limbus outlines as well as the position of the eyelids [3]. Nowadays, these parameters are often estimated from digital images or video sequences utilising image processing techniques.

Most of the pupillometers that are commercially available do not possess the capability of estimating the limbus. Relating the pupil to the limbus is possible in videokeratoscopy [4], although this technique is not reliable for eyes that have dark irides [5]. In customised refractive surgery, on the other hand, there are some commercial eye-trackers that can determine the pupil parameters and relate them to the limbus [6]. However, their accuracy has not been fully

established. Also, since they are integral parts of the excimer laser systems, they cannot be used independently.

With the introduction of high resolution CMOS imaging devices and the developments in high-speed filming it is now possible to observe the changes in pupil size during an eye-blink or sudden changes in the lighting conditions. It is known that the pupil changes its size under different lighting conditions. However, with changes in pupil dimension the pupil centre often moves in relation to other ocular landmarks [7, 8]. Such detailed observations provide clinicians and vision scientists with valuable information on eye dynamics.

Several image processing techniques devoted to pupillometry have been reported [9, 10]. Recently, a robust method for estimating the considered parameters of the anterior eye has been proposed [11]. The procedure utilises several customised image processing techniques and is reported to perform well for a wide range of clinical images. In summary, the procedure first finds the initial centre of the eye [12]. Then the limbus outline algorithm is performed in which it is crucial to determine the so-called *limbus sectors*, the area of an image that contains the transition from the limbus to the sclera. The limbus sectors depend on the characteristics of the individual eye and its direction of gaze. Figure 1 shows an example of this for a natural gaze. Next, a pupil outline algorithm is performed. The detected candidate points of the limbus and pupil are then used to estimate the parameters of the pupil and limbus models. A circle and an ellipse are the most popular models. In some cases, however, more detailed analysis of the pupil may be necessary for which one can utilise a model based on the Fourier series [13]. The whole procedure is iterated until the estimates of the pupil and limbus centers converge to stationary values.

Our goal was to extend the methodology from [11] to high speed pupillometry. In particular, we are interested in the determination of the limbus sectors that may change from one frame to the other during an eye blink.

The paper is organised as follows. In the next section, we provide details on high-speed image acquisition and intro-

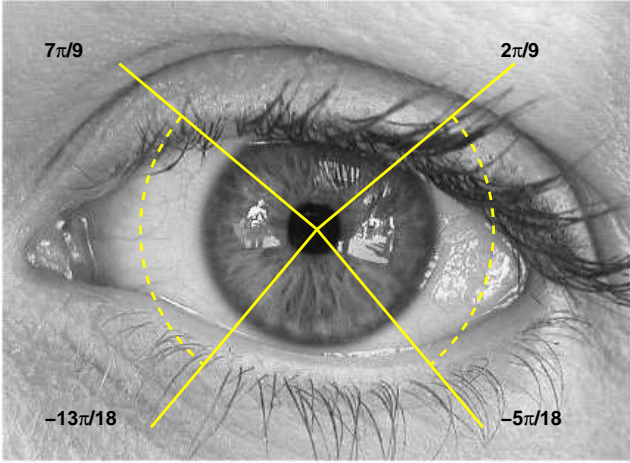


Figure 1. The image of the eye with two initial limbus sectors superimposed. The initial origin $(x_0^{(0)}, y_0^{(0)})$ is determined by the QSI detector.

duce the proposed algorithm for setting the limbus sectors. Section 3 presents an example of high-speed pupillometry during an eye blink.

2. Methodology

The high-speed camera that is used in the study is a CMOS sensor type Redlake MotionPro with a full resolution of 1280×1024 pixels. During image acquisition, the subject was asked to blink. The images were taken with the sampling rate set to 250 frames per second (FPS) under powerful 300W back-light that has been diffused through a white board. This was necessary because the CMOS camera requires a significant amount of light for image capture. A total number of 64 frames (256ms) for a full blink were then edited from the video sequence. This corresponds to the length of a typical blink. An example of eight consecutive frames taken during the first phase of the blink is shown in Figure 2. It is clear that the information on the pupil and limbus significantly change from one frame to the next. Thus, it is crucial to estimate the limbus sectors individually for each of the images in the video sequence.

2.1. Algorithm for Limbus Sector Detection

The automatic pupillometry algorithm from [11] together with our proposed automatic limbus sector estimation for high-speed digital images is used. The procedure starts with the acquisition of the first image of the eye. It is assumed that the first image from the set of considered

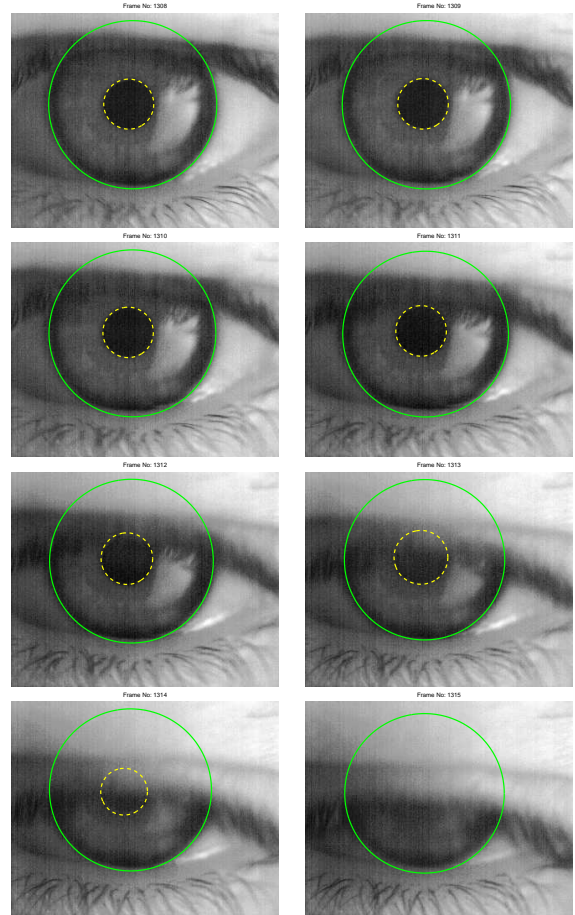


Figure 2. Eight consecutive frames in the first phase of the blink with the estimated pupil (dashed line) and limbus (solid line) outlines.

frames depicts an open eye and that it contains at least partial information on both iris and pupil.

The initial centre of the pupil $(x_0^{(0)}, y_0^{(0)})$, is determined by applying the QSI detector proposed in [12]. During the eye-blink, the eye moves slightly. However this movement does not significantly affect the performance of the QSI detector. Thus, in order to reduce the computational expense, the initial estimated centre location from the first frame is used for the rest of the 63 frames in the image pre-processing stage.

In this stage, each image is cropped to a maximum possible square inscribed in the original image and centred at $(x_0^{(0)}, y_0^{(0)})$. The cropped image should contain the whole area of the pupil and iris, and partial information on the sclera and eyelids.

Let $I(x, y)$, $x = 1, \dots, n_x$, $y = 1, \dots, n_y$ be the intensity of a grey scale image, where n_x and n_y denote the

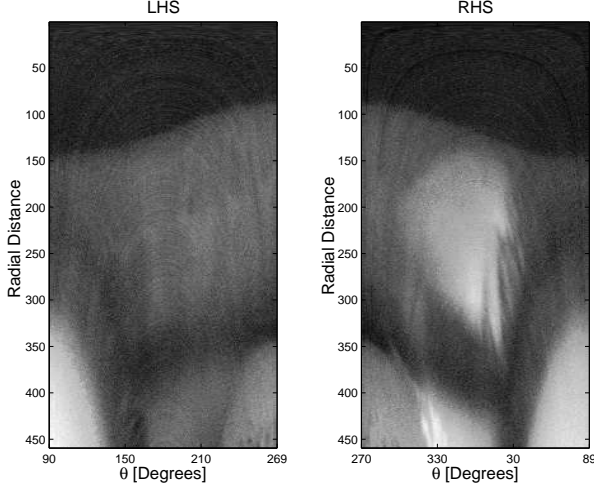


Figure 3. The polar image representation for the left and right hand sides of a typical image depicting an open eye.

number of pixels in the cropped image in the x and y directions respectively. We define a radial image profile $I_p(r, \theta)$, $r = 1, \dots, r_{\max}, \theta = \theta_{\min}, \theta_{\min} + \delta_\theta, \theta_{\min} + 2\delta_\theta, \dots, \theta_{\max}$, where δ_θ is a predetermined angular step (1 degree). We can then form an $n_r \times n_\theta$ polar-grid matrix (image) with columns corresponding to sampled radial profiles

$$\mathbf{I}_p = \begin{bmatrix} I_p(1, \theta_{\min}) & \cdots & I_p(1, \theta_{\max}) \\ I_p(2, \theta_{\min}) & \cdots & I_p(2, \theta_{\max}) \\ \vdots & \vdots & \vdots \\ I_p(r_{\max}, \theta_{\min}) & \cdots & I_p(r_{\max}, \theta_{\max}) \end{bmatrix}$$

where $n_r = r_{\max}$ and $n_\theta = (\theta_{\max} - \theta_{\min})$ [4, 11].

In the next step, two polar images are generated for the left (from 270° to 89°) and right (from 90° to 269°) hand side of each of the cropped images. An example of the polar image representation is shown in Figure 3. We note that the eyelid information appears only at the bottom of the polar image. To detect the upper and lower eyelid, we only process the section of the image that possibly contains the eyelids. Let \mathbf{I}_s be the considered section of the polar image \mathbf{I}_p ,

$$\mathbf{I}_s = \begin{bmatrix} I_s(r_s, \theta_{\min}) & \cdots & I_s(r_s, \theta_{\max}) \\ \vdots & \vdots & \vdots \\ I_s(r_{\max}, \theta_{\min}) & \cdots & I_s(r_{\max}, \theta_{\max}) \end{bmatrix}$$

where r_s to r_{\max} is a predetermined radial section that includes significant amount of the eyelid information, normally chosen to be $r_s > 0.9r_{\max}$.

To detect the angular location of upper and lower eyelid, we first average the angular intensity

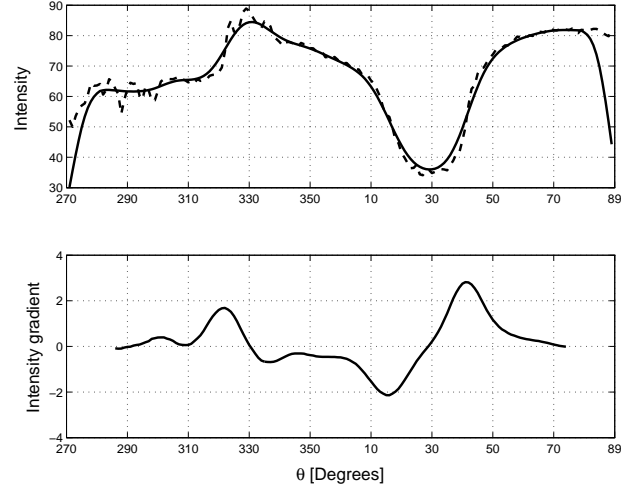


Figure 4. The average angular intensity profile before and after smoothing (top) and its derivative (bottom).

$$\bar{I}_s = \frac{1}{r_{\max} - r_s} \left[\sum_{r=r_s}^{r_{\max}} I_s(r, \theta_{\min}) \cdots \sum_{r=r_s}^{r_{\max}} I_s(r, \theta_{\max}) \right],$$

an example of which is shown by a dashed line in Figure 4. This is further smoothed with an n -point Hamming window (typically $n = 21$). The solid lines in Figure 4 show the corresponding average angular intensity profile after smoothing and its derivative. The two highest peaks are the angular location for lower θ_1 or upper θ_2 eyelid respectively. From this, the start sector and the sector size for the pupil and limbus estimation can be calculated. In this case, we determined $\theta_1 = 324^\circ$ and $\theta_2 = 42^\circ$, which are around the angular positions of the upper and lower eyelids of the right hand side of the polar image from Figure 3. We check whether the image does contain a sufficient amount of information for estimating the pupil and limbus outlines by comparing the difference of θ_1 and θ_2 with a certain threshold.

In the case where there are more than two peaks detected, the angular location that produces a smaller sector size is selected. This is done because for automatic pupillometry, it is preferable to select the part of the image without too much obstruction from the eyelashes. Further detail of automatic pupillometry can be found in [11].

3. Results

Consider the sequence of images shown in Figure 2. We run the pupillometry procedure of [11] enhanced by the au-

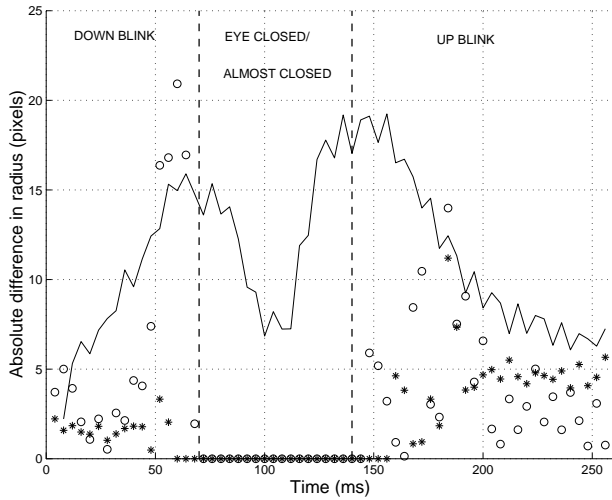


Figure 5. The absolute difference between the manual and automatic pupil (*) and iris (o) radii. The image time gradient is superimposed with the solid line.

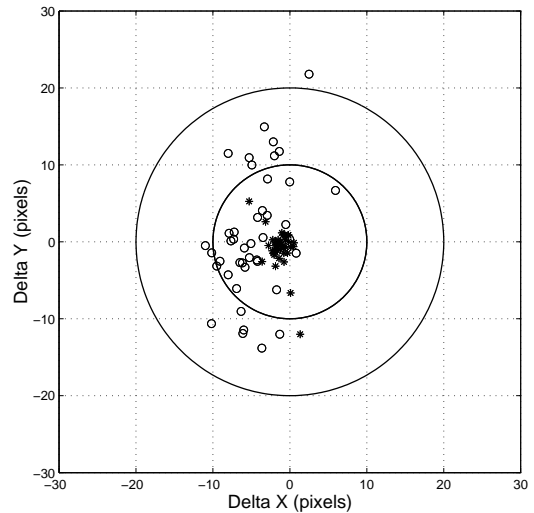


Figure 6. The difference between the manually and automatically estimated pupil (*) and limbus (o) centers.

automatic detection of limbus sectors as outlined in the previous section. The result of the estimated pupil and limbus outlines is superimposed in Figure 2 with a dashed line and a solid line, respectively.

To determine the relative accuracy of the proposed automatic methodology, we have developed a graphic user interface to assist manual fitting of the limbus and pupil. A single frame is displayed at a time and an operator is instructed to click with the mouse on 16 points that are believed to constitute the limbus outline and a further eight points for the pupil outline. The algorithm uses the manually selected points to estimate the parameters of the best-fit circle (Least Squares) for both the limbus and the pupil.

The results of two experienced operators have been averaged and compared to the fully automatic procedure. In Figure 5, we show the absolute difference between the manually and automatically estimated pupil (asterisks) and iris (circles) radii. The averaged and scaled image time gradient, i.e.

$$s \sum_{(x,y)} [I(x,y;t) - I(x,y;t-1)], \quad 0 < s < 1,$$

is superimposed with the solid line, showing the dynamic changes in the video sequence. Note that the down phase of the blink is faster than the up blink phase (76ms vs 100ms). From Figure 5, we can note that the standard deviations of the estimated limbus parameters are around three times larger than the corresponding standard deviations of the pupil parameter estimators. The deviation of limbus estimate becomes more significant towards the end of down

blink phase and the beginning of the up blink phase.

One may expect higher standard deviation for the limbus parameter estimators because, in general, the transition from the iris to sclera is not as clear as the transition from the pupil to the iris. Also, other factors such as shadowing caused by eyelashes and build-up of the tear film at the eyelid margins may contribute to a larger variability in the parameter estimates.

In Figure 6, we show the difference between the manually and automatically estimated pupil and limbus centers, denoted by asterisks and circles, respectively. Most of the pupil centres were estimated both manually and automatically within ± 4 pixels. This corresponds to approximately 100 microns. For limbus center estimation, most of the result were within ± 15 pixels (375 microns). Note however, that these results are relative to subjective measurements and show only how closely the automatic pupillometry procedure can mimic a human operator.

It is clear that both centers are slightly biased to the left. This is because the images from Figure 2 were taken with a setup consisting of a back-light located to the right of the subject. This resulted in irregular illumination of the acquired images and an unwanted reflection in the iris.

4. Conclusions

We have developed a novel procedure for estimating the limbus sectors. The proposed procedure is used with the recently proposed automatic pupillometry algorithm for the study of pupil dynamics in high speed filming. It was found

that the procedure closely mimics an experienced human operator and provides, in most cases, consistent results. It should be emphasised that the proposed methodology will be significantly hindered if the acquired images are taken with a low resolution camera. The procedure could be significantly enhanced if colour images were available [14]. In such a case, separation of features not related to the eye in the image can be achieved.

5. Acknowledgment

The project was supported by the QUT Strategic Collaborative Program scheme.

References

- [1] Holladay, J. T. "The high cost of inaccurate pupillometry," *Review of Ophthalmology*, vol. 9, no. 3, pp. 47–49, 2002.
- [2] Langenbucher, A., Seitz, B., Kus, M. M., Vilchis E. and Naumann, G. O. H. "Graft decentration in penetrating keratoplasty: nonmechanical trephination with the excimer laser (193 nm) versus the motor trephine," *Ophthalmic Surgery and Lasers*, vol. 29, no. 2, pp. 106–113, 1998.
- [3] A. D. A. Souza, E. E. S. Ruiz, and A. A. V. Cruz. "Palpebral fissure morphology segmentation and measurement using image processing," *IEEE Engineering in Medicine and Biology Magazine*, pages 114–119, January/February 2000.
- [4] Morelande, M. R., Iskander, D. R., Collins, M. J., and Franklin, R. "Automatic estimation of corneal limbus in videokeratoscopy," *IEEE Transactions on Biomedical Engineering*, vol. 49, no. 12, pp. 1617–1625, 2002.
- [5] Fogla, R. and Rao, S. K. "Pupillometry using videokeratography in eyes with dark brown irides," *Journal of Cataract and Refractive Surgery*, vol. 26, no. 9, pp. 1266–1267, 2000.
- [6] Schwiegerling, J. and Snyder, R. W. "Eye movement during laser in situ keratomileusis," *Journal of Cataract and Refractive Surgery*, vol. 26, no. 3, pp. 345–351, 2000.
- [7] Walsh, G. "The effect of mydriasis on the pupillary centration of the human eye," *Ophthalmic and Physiological Optics*, vol. 8, no. 4, pp. 178–182, 1988.
- [8] Wilson, M. A. and Campbell, M. C. W. "Change of pupil centration with change of illumination and pupil size," *Optometry and Vision Science*, vol. 698, no. 24, pp. 129–136, 1989.
- [9] Barry, J. C., Pongs, U. M., and Hillen, W. "Algorithm for Purkinje images I and IV and limbus centre localization," *Computers in Biology and Medicine*, vol. 27, no. 6, pp. 515–531, 1997.
- [10] Miro, I., Lopez-Gil, N., and Artal, P. "Pupil-meter and tracking system based in a fast image processing algorithm," *Proceedings of SPIE*, vol. 3591, pp. 63–70, 1999.
- [11] Iskander, D. R., Collins, M. J., Mioschek, S., and Trunk, M. "Automatic pupillometry from digital images," *IEEE Transactions on Biomedical Engineering*, (in review).
- [12] Iskander, D. R., Mioschek, S., Trunk, M. and Werth, W. "Detecting eyes in digital images," In *Proceeding of Seventh International Symposium on Signal Processing and Its Applications*, Vol. II, pp. 21–24, Paris, France, July 2003.
- [13] Wyatt, H. J. "The form of the human pupil," *Vision Research*, vol. 35, no. 14, pp. 2021–2036, 1995.
- [14] Chai, D. and Ngan, K. N. "Face segmentation using skin-color map in vediohone applications," *IEEE Transactions on Circuits and System for Video Technology*, vol. 9, no. 4, pp. 551–564, 2002.